Supplementary Material

Tube-Based Model Reference Adaptive Control for Vibration Suppression of Active Suspension Systems

Appendix A
Literature Review

Suspension systems can be categorized into passive, semi-active, and active suspensions. With the traditional dampers and springs installed between the sprung and unsprung masses, passive suspensions have been found unreliable systems to simultaneously provide the desired ride comfort and road-handling performances [1]. On the contrary, although semi-active suspensions have demonstrated considerable improvements over the passive ones by taking advantage of variable dampers and/or other variable dissipation parts, some limitations still remain with their ride comfort improvement capabilities [2], [3]. In contrast, active suspensions equip the system with controlled actuators placed between the sprung and unsprung masses capable of adding and dissipating energy from the system in the case of necessity to achieve specific desired performance objectives [4]. Compared with passive and semi-active suspensions, the mounted actuators help the active suspensions produce active control force to impede the road-surface-arisen vibrations and hence, provide simultaneous ride comfort and road-handling performance [5], [6].

Although active suspensions are known as effective systems to improve the vehicle dynamics performance, achieving the desired performance is yet a demanding issue to be handled. In this context, an extensive range of conventional and advanced control techniques have been developed to ensure concurrent passenger comfort and road handling such as adaptive control strategies [7], [8], adaptive neural network output feedback optimized control [9], fuzzy logic systems control methods [10], [11], conventional optimal strategies [12], [13], model predictive control [14], and sliding mode control strategies [15], [16]. Authors in [13] developed an intelligent proportional-derivative (PD) control method to attenuate the vibrations caused by road disturbance. However, despite its superior performance over linear quadratic regulator (LQR) and active disturbance rejection control, it has failed to fulfill the requirements for ride comfort, showing a weak body displacement attenuation performance. A robust sliding mode control scheme was developed in [16] to improve the ride quality and overcome road disturbances. Although the method has been reported effective, it lacks a good trade-off between passenger comfort and vertical displacement decrement. Authors in [7] developed an adaptive backstepping control to cope with the control problem of active suspension systems. Although the method was reported to deliver a desirable passenger ride comfort, it failed to provide a good road holding capability. Another work [8] investigated an adaptive backstepping-based control strategy to improve vehicle ride comfort with mechanical elastic wheels. However, although the control method was reported effective, the improvements were limited, and more efforts are yet to be done to achieve the desired ride comfort and road handling. Therefore, since the ride comfort and safety constraints on a suspension system are conflicting, improving the former leads to the latter's degradation, negatively affecting the chassis layout, and then deteriorates vehicle handling stability. Hence, it is not straightforward to make a trade-off between the two objectives as a comfort-oriented suspension should have low damping of the sprung mass to provide satisfactory isolation. Accordingly, developing effective control strategies capable of simultaneous guaranteeing ride comfort, road holding, and suspension safety is still a challenging and interesting issue to be investigated.

Adaptive control strategies are developed to deal with systems with uncertain and/or time-varying parameters by employing a control law whose parameters are tuned to match the reference system under control. Amongst the adaptive control approaches, model reference adaptive control (MRAC) provides an efficient design procedure by a well-defined reference system to be followed. Benefiting from a well-established mathematical proof of stability, the MRAC scheme compares the system's output with a stabilized reference model and regulates the controller's parameters to stabilize the overall dynamics of a feedback control system [17], [18]. Motivated by the desirable performance of the MRAC approach, various literature studies have investigated its performance in diverse linear and nonlinear practical systems [19]–[21]. An MRAC-based control scheme was proposed in [19] for control of surface-installed permanent magnet synchronous motor drives. The investigated method comprised an adaptive control term to compensate the uncertain model parameters and a stabilizing feedback control term to asymptotically stabilize the error dynamics. As the authors reported, the proposed paradigm outperformed the non-adaptive model reference control method in terms of transient response, tracking precision, and robustness against parameter uncertainties. Authors in [20] developed an initialized MRAC scheme to deal with the angular position control of a lower limb exoskeleton system. Compared to the conventional MRAC, the developed method was reported to deliver superior convergence speed and error mitigation performance. A predictive optimization-based MRAC scheme was proposed in [21] to dynamic positioning of an actuated underwater vehicle. As the authors reported through comparative investigations with conventional linear reference model-based methods, the investigated approach demonstrated superior performance under dynamic uncertainties and actuator saturations in the system.

Appendix B
Stability Analysis

To investigate the closed-loop stability, let us consider the following Lyapunov function candidate:

$$V(t) = e^T(t)Pe(t) + \frac{1}{2}tr\left[\tilde{\Psi}_1^T M^{-1}\tilde{\Psi}_1\right] + \frac{1}{2}tr\left[\tilde{\Psi}_{eq}^T M^{-1}\tilde{\Psi}_{eq}\right] \quad (1)$$

where $P \in \Re^{n\times n}$ is a positive definite symmetric matrix and $tr[\cdot]$ denotes the trace of the matrix.

A positive definite matrix $Q \in \Re^{m\times m}$ can be defined such that

$$M = \Psi_{eq}^* Q = \left(\Psi_{eq}^* Q\right)^T = Q^T \Psi_{eq}^{*T} > 0. \quad (2)$$

where $\Psi_{eq}^* = \Psi_2^* + \Psi_c^*$.

Differentiating (1) with respect to time yields

$$\dot{V}(t) = \dot{e}^T(t)Pe(t) + e^T(t)P\dot{e}(t) + tr\left[\dot{\tilde{\Psi}}_1^T M^{-1}\tilde{\Psi}_1\right] + tr\left[\dot{\tilde{\Psi}}_{eq}^T M^{-1}\tilde{\Psi}_{eq}\right]. \quad (3)$$

Substituting $\dot{e}(t) = A_r e(t) + B\tilde{\Psi}_1^T\Gamma(t) + B\tilde{\Psi}_{eq}\upsilon_r(t)$ into (3), we have

$$\begin{aligned}\dot{V}(t) = &\left[e^T(t)A_r^T + \Gamma^T(t)\tilde{\Psi}_1 B^T + \upsilon_r^T(t)\tilde{\Psi}_{eq}^T B^T\right]Pe(t) \\ &+ e^T(t)P\left[A_r e(t) + B\tilde{\Psi}_1^T\Gamma(t) + B\tilde{\Psi}_2 r(t) + B\tilde{\Psi}_c\upsilon_c(t)\right] \\ &+ tr\left[\dot{\tilde{\Psi}}_1^T M^{-1}\tilde{\Psi}_1\right] + tr\left[\dot{\tilde{\Psi}}_{eq}^T M^{-1}\tilde{\Psi}_{eq}\right].\end{aligned} \quad (4)$$

Equation (4) can be rewritten in the following form:

$$\begin{aligned}\dot{V}(t) = &e^T(t)\left(A_r^T P + PA_r\right)e(t) + 2e^T(t)PB\tilde{\Psi}_1\Gamma(t) \\ &+ 2e^T(t)PB\tilde{\Psi}_{eq}\upsilon_r(t) + tr\left[\dot{\tilde{\Psi}}_1^T M^{-1}\tilde{\Psi}_1\right] + tr\left[\dot{\tilde{\Psi}}_{eq}^T M^{-1}\tilde{\Psi}_{eq}\right].\end{aligned} \quad (5)$$

Choosing P satisfying $A_r^T P + PA_r = -L$, where L is a positive

definite matrix, yields

$$\dot{V}(t) = -e^T(t)Le(t) + 2e^T(t)PB\tilde{\Psi}_1\Gamma(t) + 2e^T(t)PB\tilde{\Psi}_{eq}\upsilon_r(t) + tr\left[\dot{\tilde{\Psi}}_1^T M^{-1}\tilde{\Psi}_1\right] + tr\left[\dot{\tilde{\Psi}}_{eq}^T M^{-1}\tilde{\Psi}_{eq}\right]. \quad (6)$$

Since L is positive definite, $-e^T(t)Le(t)$ is always non-positive. As a result, to realize $\dot{V}(t) \le 0$ indicating the stability of the closed-loop system, the following relationships must be established:

$$tr\left[\dot{\tilde{\Psi}}_1^T M^{-1}\tilde{\Psi}_1\right] = -2e^T(t)PB\tilde{\Psi}_1\Gamma(t) \quad (7a)$$

$$tr\left[\dot{\tilde{\Psi}}_{eq}^T M^{-1}\tilde{\Psi}_{eq}\right] = -2e^T(t)PB\tilde{\Psi}_{eq}\upsilon_r(t). \quad (7b)$$

Considering the foregoing compatibility conditions, the following regulation rules can be derived:

$$\dot{\tilde{\Psi}}_1 = -2Q^T B_r Pe(t)\Gamma^T(t) \quad (8a)$$

$$\dot{\tilde{\Psi}}_{eq} = -2Q^T B_r^T Pe(t)\upsilon_r^T(t). \quad (8b)$$

Considering $\upsilon_a(t)$, the optimization problem with the index $J = \upsilon^2(t) = (\upsilon_a(t) + \upsilon_c(t))^2$ has the following solution υ_c^{opt}:

$$\upsilon_c^{opt} = \begin{cases} -\upsilon_a(t), & \text{if } \upsilon_a(t) \in [\upsilon_c^-, \upsilon_c^+] \\ \arg\min\left(J(\upsilon_c^-, \upsilon_c^+)\right), & \text{if } \upsilon_a(t) \notin [\upsilon_c^-, \upsilon_c^+] \end{cases} \quad (9)$$

where $J(\upsilon_c^+)$ and $J(\upsilon_c^-)$ represent the values of J for $\upsilon_c(t) = \upsilon^+$ and $\upsilon_c(t) = \upsilon^-$, respectively. Accordingly, the controller $\upsilon(t)$ guarantees that the tracking error tends to zero with minimized control cost. ■

APPENDIX C
T-MRAC DESIGN FOR THE QUARTER-CAR SUSPENSION SYSTEM

Let us consider the following quarter-car suspension reference model for the T-MRAC design:

$$\dot{\Gamma}_r(t) = A_r\Gamma_r(t) + B_{r1}\upsilon_r(t) + B_{r2}\dot{z}_r = A\Gamma(t) + B_1 f_a + B_2\dot{z}_r \quad (10)$$

where $B_1 \in \Re^{n\times 1}$ and $B_2 \in \Re^{n\times 1}$.

Defining $e(t) = \Gamma(t) - \Gamma_r(t)$, the dynamic equation of error can be described as

$$\dot{e}(t) = A\Gamma(t) + B_1 f_a + B_2\dot{z}_r - A_r\Gamma_r(t) - B_{r1}\upsilon_r(t) - B_{r2}\dot{z}_r. \quad (11)$$

Assuming $B_{r2} = B_2$ and $B_{r1} = B_1\Psi_c^*$ we have

$$\dot{e}(t) = \left(A_r - B_1\Psi_1^{*T}\right)\Gamma(t) + B_1 f_a - A_r\Gamma_r(t) - B_{r1}\upsilon_r(t) = A_r e(t) - B_1\Psi_1^{*T}\Gamma(t) + B_1 f_a - B_{r1}\upsilon_r(t). \quad (12)$$

Considering $\upsilon_r(t) = r(t) + \upsilon_c(t)$, (12) can be rewritten as

$$\dot{e}(t) = A_r e(t) - B_1\Psi_1^{*T}\Gamma(t) + B_1 f_a - B_{r1}r(t) - B_{r1}\upsilon_c(t). \quad (13)$$

If the control law f_a is adopted as $f_a(t) = \upsilon_a(t) + \upsilon_c(t)$, then we have

$$\dot{e}(t) = A_r e(t) - B_1\Psi_1^{*T}\Gamma(t) + B_1\upsilon_a(t) + B_1\upsilon_c(t) - B_1\Psi_c^* r(t) - B_1\Psi_c^*\upsilon_c(t). \quad (14)$$

Defining $\Phi(t) = \begin{bmatrix} \Gamma(t) & r(t) \end{bmatrix}^T \in \Re^{(n+m)\times 1}$ yields

$$\dot{e}(t) = A_r e(t) + B_1\left[\upsilon_a(t) - \Psi^{*T}\Phi(t) - \Psi_c^*\upsilon_c(t)\right] \quad (15)$$

where $\Psi^{*T} = \begin{bmatrix} \Psi_1^{*T} & \Psi_c^* \end{bmatrix} \in \Re^{m\times(n+m)}$.

It is noteworthy that the Lyapunov-based stability analysis can be achieved with the same procedure as stated in Appendix B.

APPENDIX D
CONSIDERED ROAD PROFILES

Three different road profiles are considered in this study to simulate different practical road situations, namely the bump-dip road, random road, and sinusoidal profiles. Simulations are carried out using MATLAB R2020a 64-bit, on a ASUS laptop with 64-bit win10 operating system, processor: Intel® core™ i7-8550U CPU 2.50 GHz, and 8.00 GB installed memory.

A. Bump-Dip Road

The considered bump-dip road profile shown in Fig. 1 is given as follows [22]:

$$z_r = \begin{cases} -0.0592t_1^3 + 0.1332t_1^2 + d(t), & 3.5 \le t < 5 \\ 0.0592t_2^3 + 0.1332t_2^2 + d(t), & 5 \le t < 6.5 \\ 0.0592t_3^3 - 0.1332t_3^2 + d(t), & 8.5 \le t < 10 \\ -0.0592t_4^3 - 0.1332t_4^2 + d(t), & 10 \le t < 11.5 \\ d(t), & \text{else} \end{cases} \quad (16)$$

where $d(t) = 0.002\sin(2\pi t) + 0.002\sin(7.5\pi t)$ represents a periodic disturbance, and $t_1 = t - 3.5$, $t_2 = t - 6.5$, $t_3 = t - 8.5$, and $t_4 = t - 11.5$.

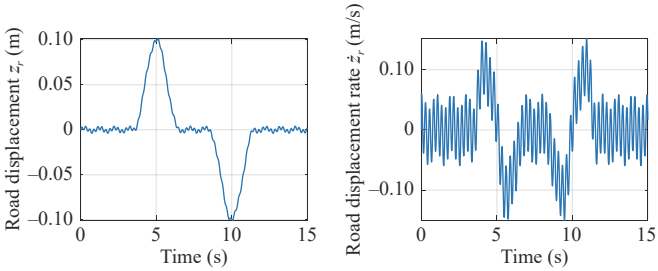

Fig. 1. The bump-dip road profile.

B. Random Road

Using the shaping filter method [23], a class C random road profile as per the international organization for standardization (ISO) 8608 [24] is considered as shown in Fig. 2.

$$\dot{z}_r = -\delta V z_r + \varpi \quad (17)$$

where V denotes the vehicle speed and ϖ is a white noise process with spectral density $\Psi_\varpi = 2\delta V\sigma^2$ (see [23] for more details). The vehicle is assumed to run at a constant speed $V = 30$ [m/s], and $\delta = 16\times 10^{-6}$ [m^3] and $\sigma = 8\times 10^{-3}$ [m] are considered [23].

C. Sinusoidal Road

The sinusoidal waveform (Fig. 3) is considered as the third road profile as follows:

$$z_r = \sum_{i=1}^{n} A_i\sin(2\pi\Omega_i t + \phi_i) \quad (18)$$

where A_i is the amplitude, Ω_i represents the wave number, and ϕ_i is the phase. The road surface parameters are considered as $n = 2$, $\phi_i = 0$, $\Omega_{1,2} = \{1, 10\}$ [Hz], and $A_{1,2} = \{0.05, 0.005\}$ [m].

APPENDIX E
MORE PERFORMANCE ANALYSIS

In order to have a more detailed substantiation on the suspension performance of the proposed T-MRAC scheme, the root mean square (RMS) values of the suspension system dynamic output are investigated as a quantitative index reflecting the extent of improvements being made. Since this index directly relates to riding comfort, it can be counted as a good benchmark to measure the suspension performance. The RMS value for a typical signal $\Theta(t)$ can be calculated as

$$RMS_{\Theta(t)} = \left(\frac{1}{N}\int_0^N \Theta^2(t)\,dt\right)^{\frac{1}{2}} \quad (19)$$

where N denotes the simulation time.

Table I lists the RMS values of the sprung vertical displacement, sprung vertical speed, and actuator force obtained under different road profiles. From Table I, it can be observed that the proposed T-MRAC approach effectively improves the ride comfort quality and

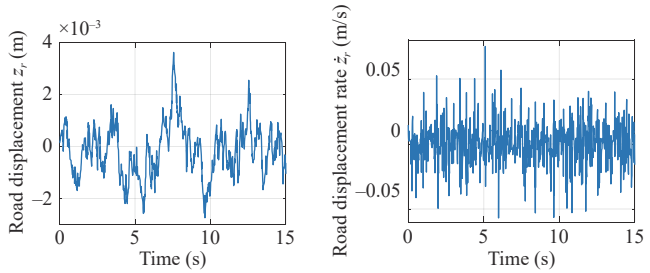

Fig. 2. The class C random road profile.

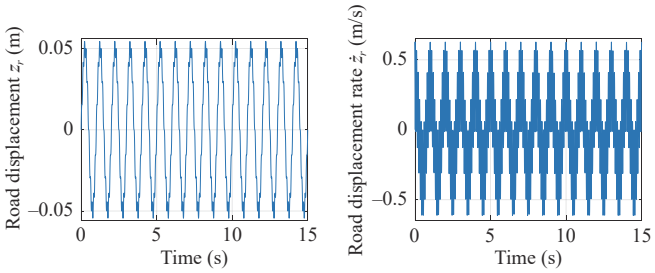

Fig. 3. The Sinusoidal road profile.

TABLE I
RMS VALUES FOR DIFFERENT ROAD PROFILES; A SUMMARY OF RESULTS

Road type		γ_1	γ_3	Actuator force
Case 1	MRAC	0.0229	0.0082	473.5629
	SMC	0.0082	0.0026	435.6792
	T-MRAC	473.5629	0.0017	388.8987
Case 2	MRAC	3.9580e-04	0.0052	48.9743
	SMC	3.1634e-05	0.0048	42.1380
	T-MRAC	1.5925e-05	0.0028	23.6611
Case 3	MRAC	0.0067	0.0877	847.2614
	SMC	5.8270e-04	0.0299	661.4036
	T-MRAC	2.8882e-04	0.0149	625.3379

reduces the road disturbance with less actuator force compared to that of MRAC and SMC approaches. The numerical results in Table I alongside the preceding results, indicate the effectiveness of the developed approach and illustrate its superior control performance.

References

[1] G. Georgiou, G. Verros, and S. Natsiavas, "Multi-objective optimization of quarter-car models with a passive or semi-active suspension system," *Vehicle System Dynamics*, vol. 45, no. 1, pp. 77–92, 2007.

[2] H. Pan, W. Sun, X. Jing, H. Gao, and J. Yao, "Adaptive tracking control for active suspension systems with non-ideal actuators," *Journal of Sound and Vibration*, vol. 399, pp. 2–20, 2017.

[3] K. El Majdoub, F. Giri, and F.-Z. Chaoui, "Adaptive backstepping control design for semi-active suspension of half-vehicle with magnetorheological damper," *IEEE/CAA J. Autom. Sinica*, vol. 8, no. 3, pp. 582–596, 2020.

[4] J. Na, Y. Huang, X. Wu, S.-F. Su, and G. Li, "Adaptive finite-time fuzzy control of nonlinear active suspension systems with input delay," *IEEE Trans. Cybernetics*, vol. 50, no. 6, pp. 2639–2650, 2019.

[5] G. I. Mustafa, H. Wang, and Y. Tian, "Vibration control of an active vehicle suspension systems using optimized model-free fuzzy logic controller based on time delay estimation," *Advances in Engineering Software*, vol. 127, pp. 141–149, 2019.

[6] C. Onat, I. Kucukdemiral, S. Sivrioglu, I. Yuksek, and G. Cansever, "LPV gain-scheduling controller design for a non-linear quarter-vehicle active suspension system," *Transactions of the Institute of Measurement and Control*, vol. 31, no. 1, pp. 71–95, 2009.

[7] H. Pang, X. Zhang, J. Chen, and K. Liu, "Design of a coordinated adaptive backstepping tracking control for nonlinear uncertain active suspension system," *Applied Mathematical Modelling*, vol. 76, pp. 479–494, 2019.

[8] Q. Wang, Y. Zhao, H. Xu, and Y. Deng, "Adaptive backstepping control with grey signal predictor for nonlinear active suspension system matching mechanical elastic wheel," *Mechanical Systems and Signal Processing*, vol. 131, pp. 97–111, 2019.

[9] Y. Li, Y. Liu, and S. Tong, "Observer-based neuro-adaptive optimized control of strict-feedback nonlinear systems with state constraints," *IEEE Trans. Neural Networks and Learning Systems*, 2021. DOI: 10.1109/TNNLS.2021.3051030.

[10] H. Pang, F. Liu, and Z. Xu, "Variable universe fuzzy control for vehicle semi-active suspension system with mr damper combining fuzzy neural network and particle swarm optimization," *Neurocomputing*, vol. 306, pp. 130–140, 2018.

[11] F. Zhang, J. Hua, and Y. Li, "Indirect adaptive fuzzy control of siso nonlinear systems with input-output nonlinear relationship," *IEEE Trans. Fuzzy Systems*, vol. 26, no. 5, pp. 2699–2708, 2018.

[12] X. Min, Y. Li, and S. Tong, "Adaptive fuzzy optimal control for a class of active suspension systems with full-state constraints," *IET Intelligent Transport Systems*, vol. 14, no. 5, pp. 371–381, 2020.

[13] M. Haddar, R. Chaari, S. C. Baslamisli, F. Chaari, and M. Haddar, "Intelligent pd controller design for active suspension system based on robust model-free control strategy," *Proc. the Institution of Mechanical Engineers, Part C: Journal of Mechanical Engineering Science*, vol. 233, no. 14, pp. 4863–4880, 2019.

[14] J. Theunissen, A. Sorniotti, P. Gruber, S. Fallah, M. Ricco, M. Kvasnica, and M. Dhaens, "Regionless explicit model predictive control of active suspension systems with preview," *IEEE Trans. Industrial Electronics*, vol. 67, no. 6, pp. 4877–4888, 2019.

[15] L. Ovalle, H. Ríos, and H. Ahmed, "Robust control for an active suspension system via continuous sliding-mode controllers," *Engineering Science and Technology, an Int. Journal*, 2021.

[16] V. S. Deshpande, B. Mohan, P. Shendge, and S. Phadke, "Disturbance observer based sliding mode control of active suspension systems," *Journal of Sound and Vibration*, vol. 333, no. 11, pp. 2281–2296, 2014.

[17] D. Zhang and B. Wei, "A review on model reference adaptive control of robotic manipulators," *Annual Reviews in Control*, vol. 43, pp. 188–198, 2017.

[18] N. Aguila-Camacho and M. A. Duarte-Mermoud, "Improving the control energy in model reference adaptive controllers using fractional adaptive laws," *IEEE/CAA J. Autom. Sinica*, vol. 3, no. 3, pp. 332–337, 2016.

[19] A. T. Nguyen, M. S. Rafaq, H. H. Choi, and J.-W. Jung, "A model reference adaptive control based speed controller for a surface-mounted permanent magnet synchronous motor drive," *IEEE Trans. Industrial Electronics*, vol. 65, no. 12, pp. 9399–9409, 2018.

[20] M. S. Amiri, R. Ramli, and M. F. Ibrahim, "Initialized model reference adaptive control for lower limb exoskeleton," *IEEE Access*, vol. 7, pp. 167 210–167 220, 2019.

[21] J. Gao, P. Wu, T. Li, and A. Proctor, "Optimization-based model reference adaptive control for dynamic positioning of a fully actuated underwater vehicle," *Nonlinear Dynamics*, vol. 87, no. 4, pp. 2611–2623, 2017.

[22] C. M. Ho, D. T. Tran, and K. K. Ahn, "Adaptive sliding mode control based nonlinear disturbance observer for active suspension with pneumatic spring," *Journal of Sound and Vibration*, p. 116241, 2021.

[23] F. Tyan, Y.-F. Hong, S.-H. Tu, W. S. Jeng, *et al.*, "Generation of random road profiles," *Journal of Advanced Engineering*, vol. 4, no. 2, pp. 1373–1378, 2009.

[24] T. C. ISO/TC, M. Vibration, S. S. S. Measurement, E. of Mechanical Vibration, and S. as Applied to Machines, *Mechanical Vibration–Road Surface Profiles–Reporting of Measured Data*, vol. 8608. Int. Organization for Standardization, 1995.